Supplementary Material

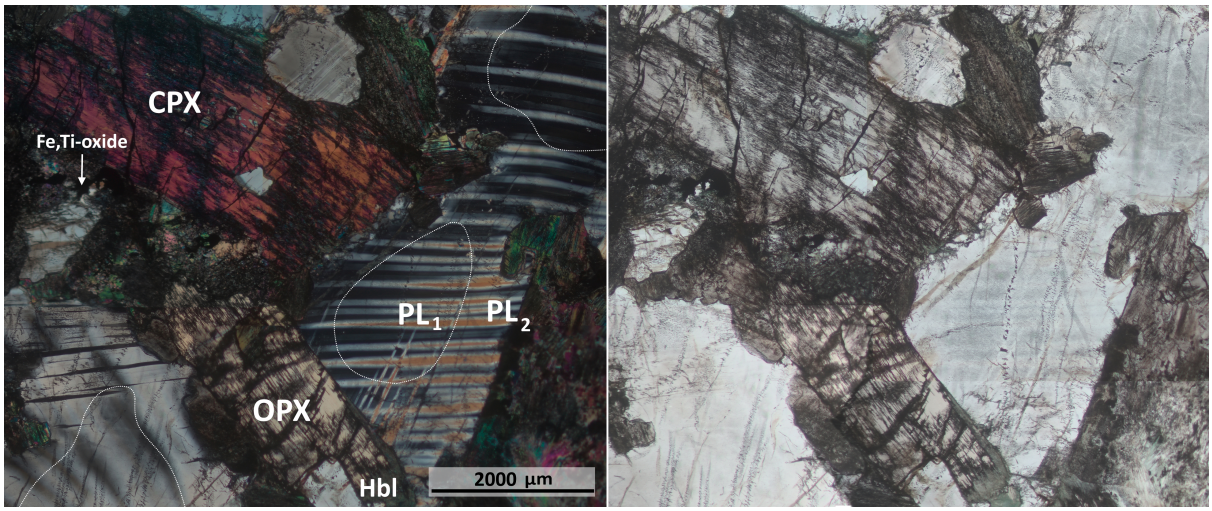

(a)

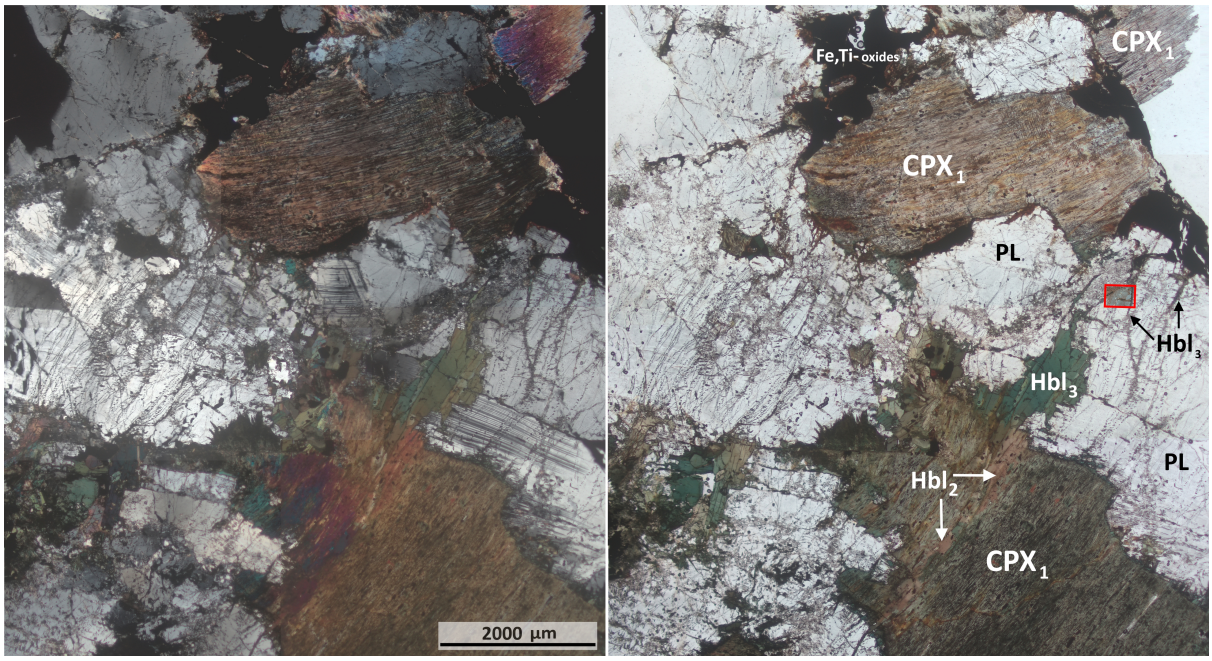

(b)

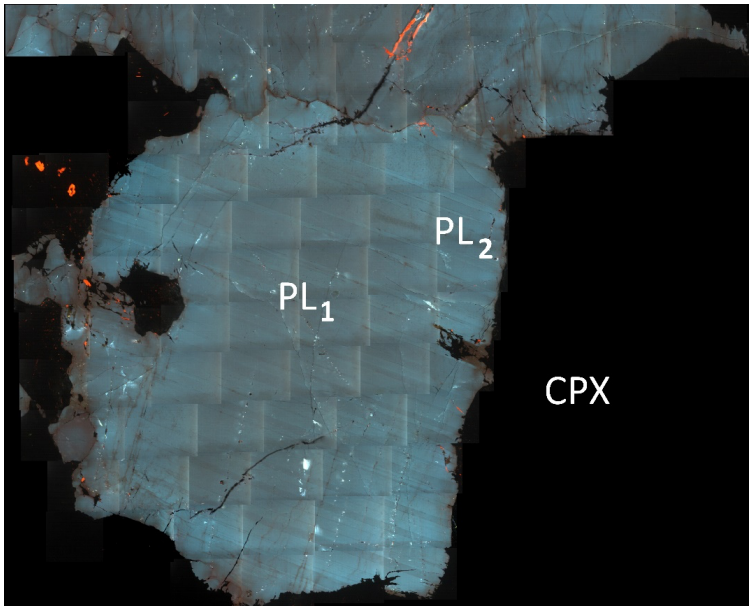

(c)

Fig. S1. Microphotographs of (a) the non-altered (Sample 277-7) and (b) altered gabbros in plane- (on the left) and cross- (on the right) polarized light. The red frame shows the area shown in the Figure S3. White dashed lines contour the areas with abundant Fe, Ti-oxide micro-inclusions in plagioclase. (c) Cathodoluminescence image of plagioclase grain in *non-altered gabbro* (Sample 277-10): core zone plagioclase (PL1) and rim zone plagioclase (PL2). CPX – clinopyroxene; OPX – orthopyroxene; CPX_1, Hbl_2 and Hbl_3 are generation of clinopyroxene and hornblend according to (Pertsev et al., 2015).

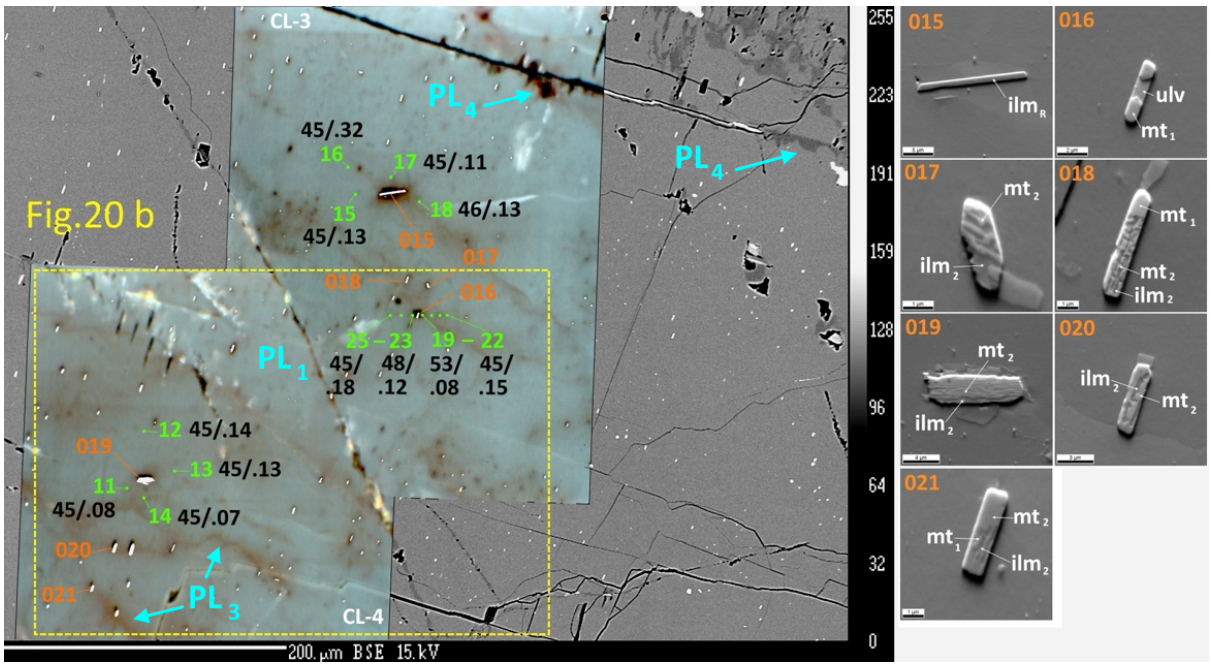

Fig. S2. Left side: CL image of a plagioclase grain from *altered gabbro*. The cracks of the hydrothermally affected plagioclase PL_3 shows reddish colour together with lined up Fe-Ti oxide micro-inclusions. Right side: SE images of individual Fe-Ti oxide micro-inclusions

hosted in the plagioclase grain shown on the left. See Fig. 1f, Fig. 2, Fig. 4d,e. Different generations of the plagioclase are shown (PL1 – PL4).

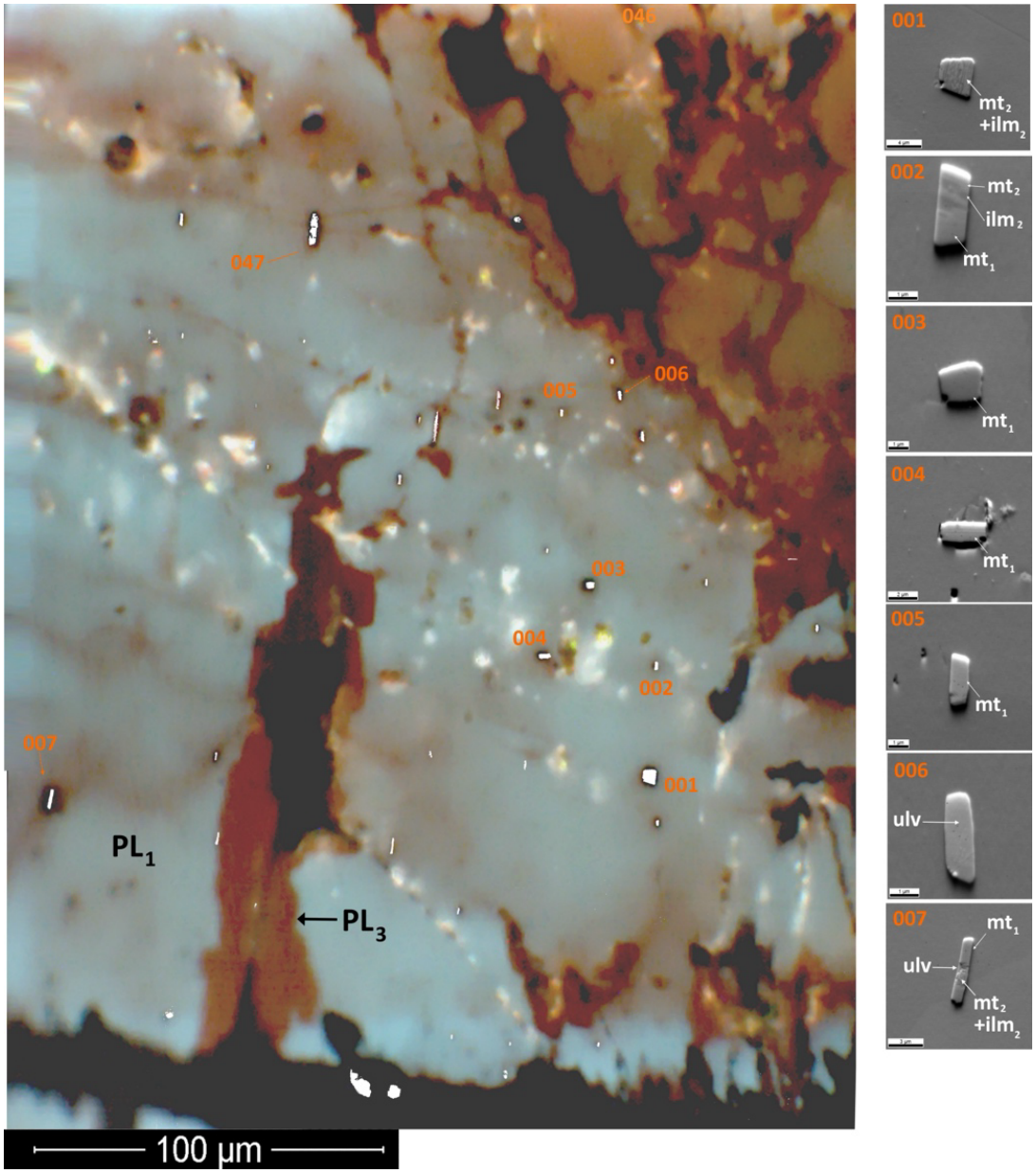

Fig. S3. Left side: Cathodoluminescence (CL) image of a plagioclase grain from the *altered gabbro*. The early magmatic plagioclase PL_1 is blueish and is almost free of the inclusions or contains dust-like inclusions. The cracks of the hydrothermally affected plagioclase PL_3 shows reddish colour. Right side: SE images of individual Fe-Ti oxide micro-inclusions hosted in the plagioclase grain shown on the left. See Fig. 4g, h.

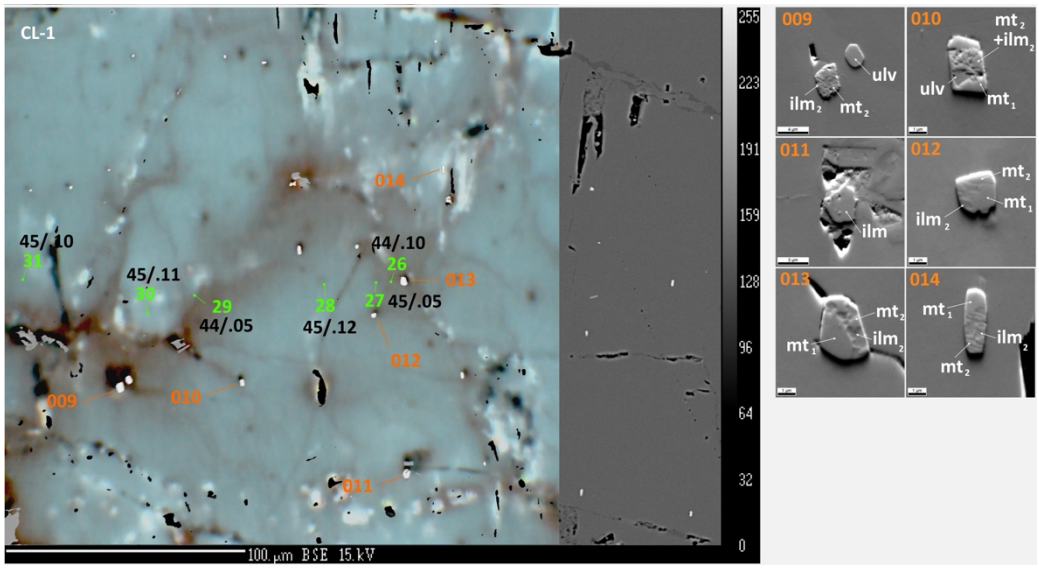

Fig. S4. Left side: CL image of a plagioclase grain from the *altered gabbro*. The cracks of the hydrothermally affected plagioclase PL_3 shows reddish colour. Right side: SE images of individual Fe-Ti oxide micro-inclusions hosted in the plagioclase grain shown on the left.

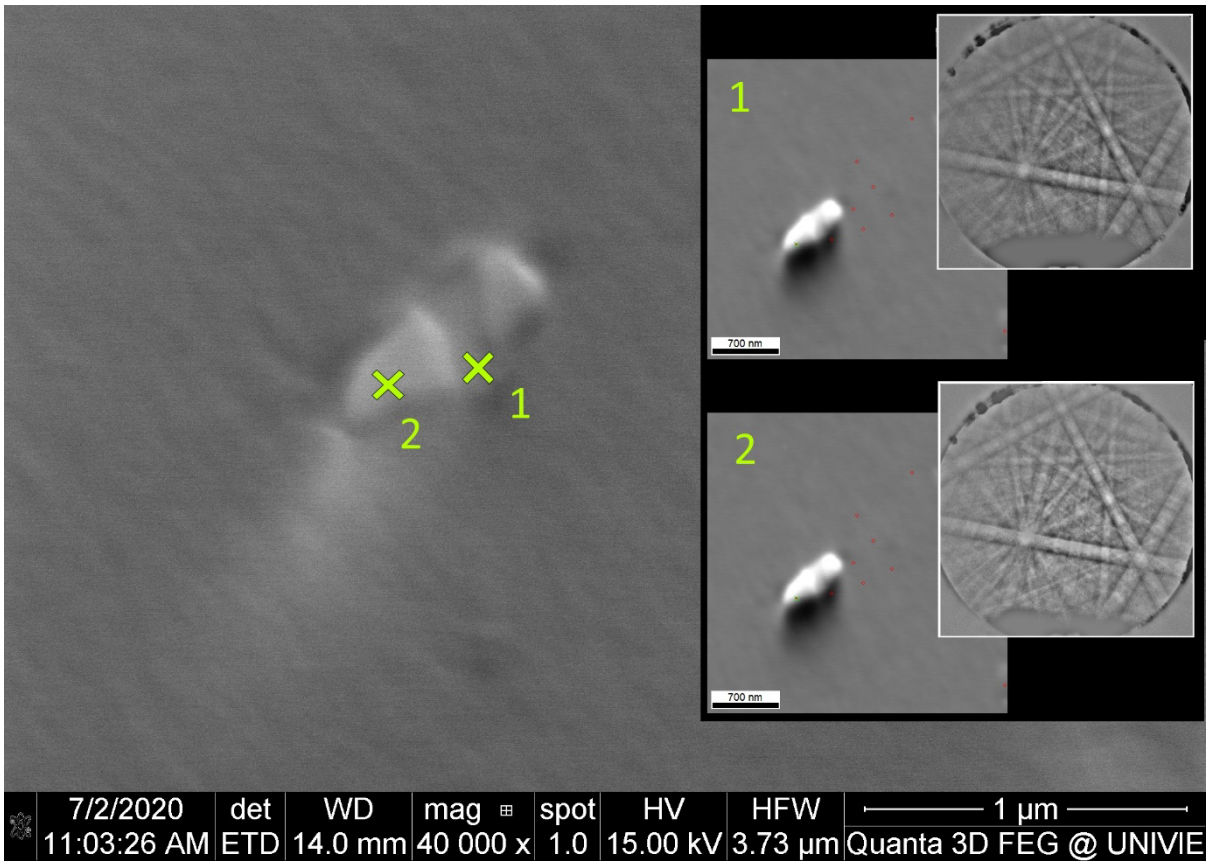

Fig. S5. The magnetite-ulvospinel inclusion in plagioclase of *non-altered gabbro*: EBSD data revealing the identical crystal structures of the magnetite matrix (2) and lamella (1).

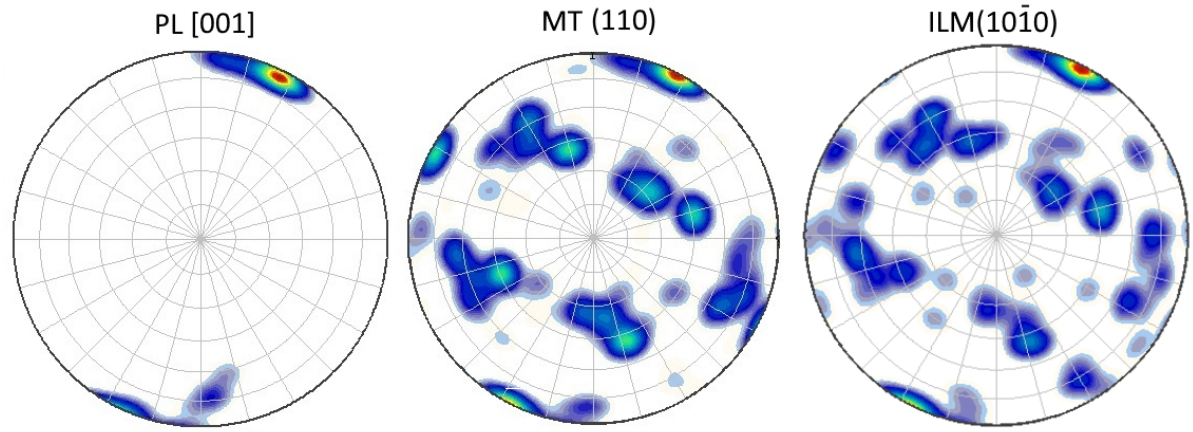

Fig. S6. Stereographic projection, derived from EBSD data, depicts the COR among PL[001]-mt (38 magnetite/ulvospinel grains) micro-inclusions, associated internal ilmenite lamellae, and the plagioclase host in the *altered gabbro*. The majority of the inclusions exhibit parallelism between one of the mt{110} plane normals and one of the ilm(10-10) plane normals with pl[001]. The plagioclase host has undergone plastic deformation, as indicated by Pertsev et al. (2015).

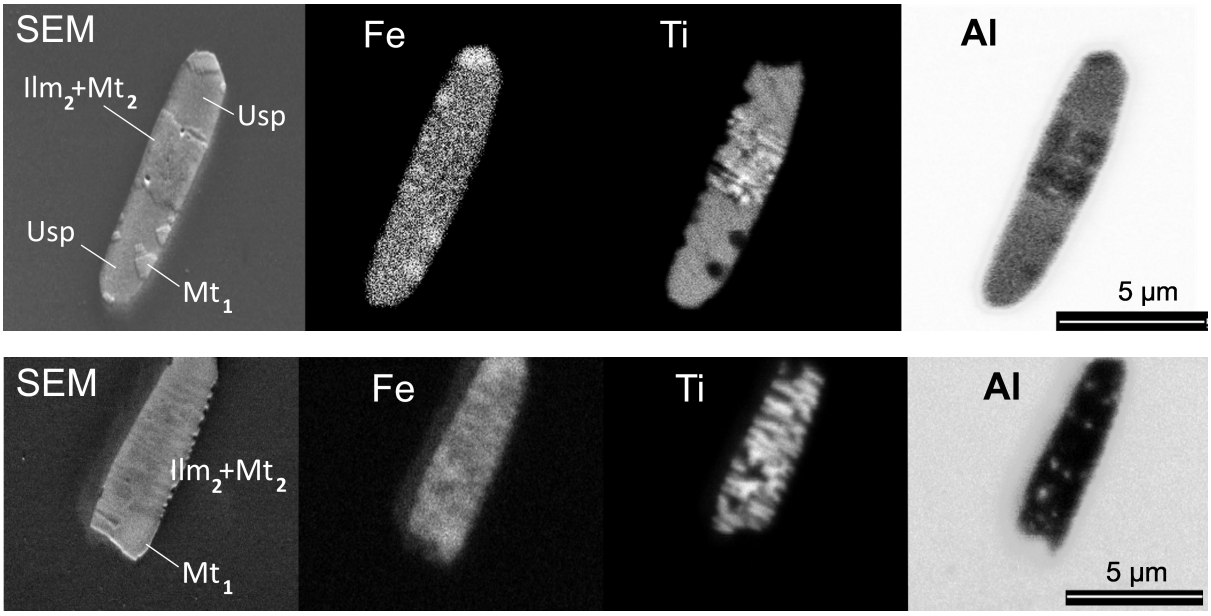

Fig. S7. Element map of the magnetite-ilmenite-ulvospinel (above) and in magnetite-ilmenite (below) inclusions hosted in plagioclase from *altered gabbro*. Al is dissolved in ulvospinel phase and absent in Mt_1 and Mt_2 (above). Al is localized in the roundish fine inclusions (obviously secondary hercynite), in the Mt_2-Ilm_2 aggregate replacing Usp (below).

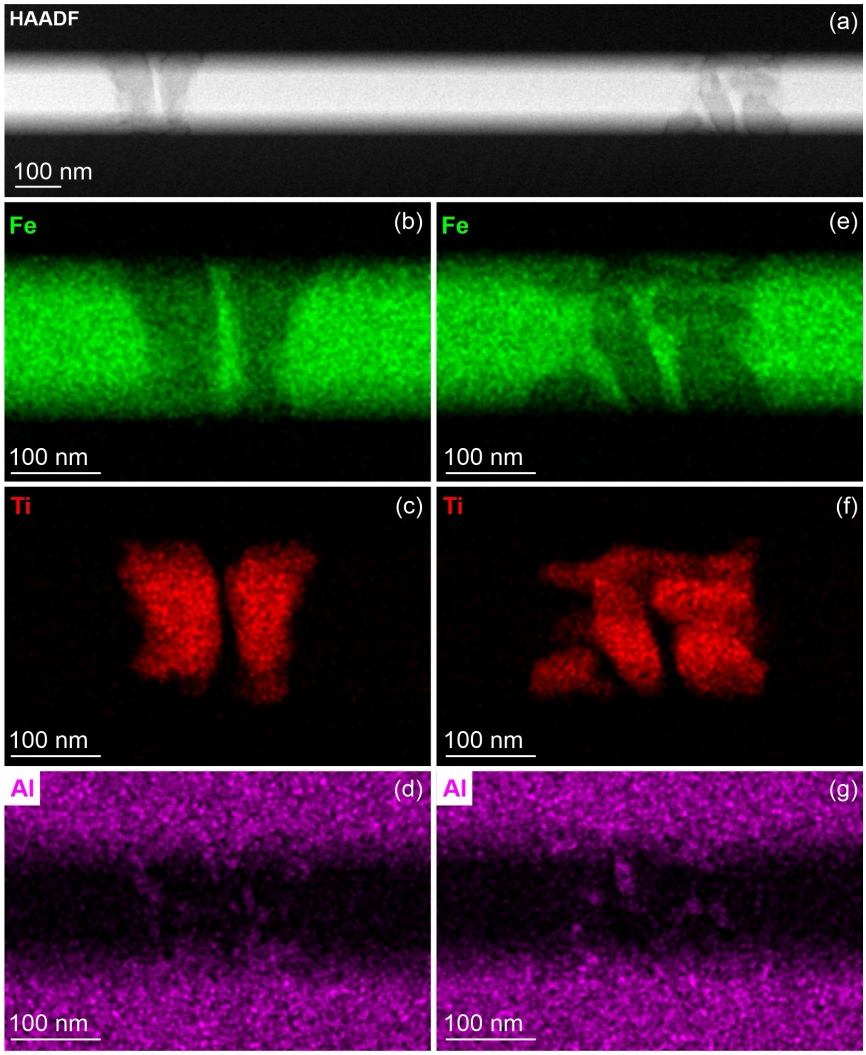

Fig. S8. (a) HAADF STEM image of a second lath shaped pl[001] type inclusion (Fig. 1e) extracted by FIB so that the inclusion elongation direction, i.e. one set of mt⟨110⟩ ‖ pl[001], is parallel to the plane of the FIB foil. The boundaries between the inclusion and the plagioclase host is inclined to the incident electron beam, and so the magnetite-plagioclase boundaries are blurred. STEM-EDS distribution maps of Fe, Ti and Al of the two segments in the inclusion under higher magnification are shown in (b-d) and (e-g), respectively. The two segments are composed of polycrystalline ilmenite in the magnetite matrix, with Al enriched at the ilmenite-magnetite interface.

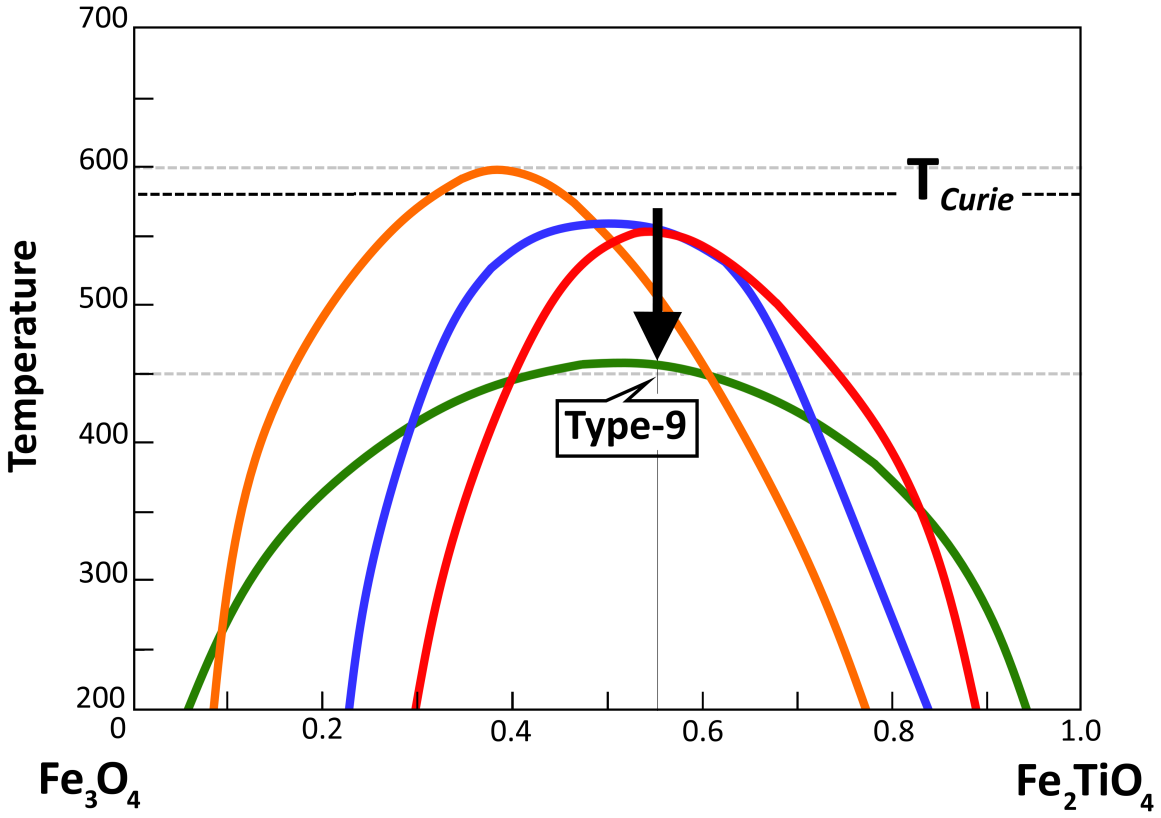

Fig. S9. Diagram of xFe$_2$TiO$_4$ versus temperature (°C) showing the experimental and schematic solvus of the magnetite–ulvospinel solid solution. The colored curves represent experimentally determined solvus boundaries from the following studies: Lilova et al. (2012) – red curve; Vincent et al. (1957) – orange curve; Price (1981) – green curve; and Lindsley (1981) – blue curve. The black arrow indicates the minimum temperature at which exsolution of Type-8 micro-inclusions occurs, resulting in the formation of two-phase magnetite-ulvospinel micro-inclusions classified as Type-9.